Protein Science (1995), *4*:1718–1729. Cambridge University Press. Printed in the USA.

The structure of *Escherichia coli* heat-stable enterotoxin b by nuclear magnetic resonance and circular dichroism

MUPPALLA SUKUMAR,[1] JOSEP RIZO,[2] MARK WALL,[3] LAWRENCE A. DREYFUS,[4] YANKEL M. KUPERSZTOCH,[5] AND LILA M. GIERASCH[1]

[1] Department of Chemistry, University of Massachusetts, Amherst, Massachusetts 01003
[2] Department of Pharmacology, [3] Howard Hughes Medical Institute, and [5] Department of Microbiology, University of Texas Southwestern Medical Center, Dallas, Texas 75235
[4] Division of Cell Biology and Biophysics, University of Missouri, Kansas City, Missouri 64110

(RECEIVED May 4, 1995; ACCEPTED June 26, 1995)

Abstract

The heat-stable enterotoxin b (STb) is secreted by enterotoxigenic *Escherichia coli* that cause secretory diarrhea in animals and humans. It is a 48-amino acid peptide containing two disulfide bridges, between residues 10 and 48 and 21 and 36, which are crucial for its biological activity. Here, we report the solution structure of STb determined by two- and three-dimensional NMR methods. Approximate interproton distances derived from NOE data were used to construct structures of STb using distance-geometry and simulated annealing procedures. The NMR-derived structure shows that STb is helical between residues 10 and 22 and residues 38 and 44. The helical structure in the region 10–22 is amphipathic and exposes several polar residues to the solvent, some of which have been shown to be important in determining the toxicity of STb. The hydrophobic residues on the opposite face of this helix make contacts with the hydrophobic residues of the C-terminal helix. The loop region between residues 21 and 36 has another cluster of hydrophobic residues and exposes Arg 29 and Asp 30, which have been shown to be important for intestinal secretory activity. CD studies show that reduction of disulfide bridges results in a dramatic loss of structure, which correlates with loss of function. Reduced STb adopts a predominantly random-coil conformation. Chromatographic measurements of concentrations of native, fully reduced, and single-disulfide species in equilibrium mixtures of STb in redox buffers indicate that the formation of the two disulfide bonds in STb is only moderately cooperative. Similar measurements in the presence of 8 M urea suggest that the native secondary structure significantly stabilizes the disulfide bonds.

Keywords: distance geometry; enterotoxin; NMR spectroscopy; secretory diarrhea

Enterotoxigenic *Escherichia coli* synthesize two types of enterotoxins, the heat-labile (LT) and heat-stable (ST) families of enterotoxins, which cause secretory diarrhea in humans and animals (Sack, 1975; Betley et al., 1986). Whereas LTs are periplasmic, STs are extracellular toxins. STs include the methanol-soluble STa and methanol-insoluble STb (Burgess et al., 1978; Whipp et al., 1981). STas are 18–19-amino acid extracellular peptides that result from two independent proteolytic cleavages on a 72-amino acid precursor (pre-pro-STa) (Rasheed et al., 1990). The mature STa contains three disulfide bridges (Gariépy et al., 1987; Shimonishi et al., 1987). The solution structure for this toxin has been determined by NMR methods and by X-ray diffraction studies (Gariépy et al., 1986; Ozaki et al., 1991). STb is also synthesized as a 71-amino acid precursor (Lee et al., 1983; Picken et al., 1983). Mature STb is a 48-amino acid peptide, with four Cys residues and no homology to STa (Dreyfus et al., 1992). The inferred N-terminus of pro-STb (residues 1–23) has characteristics of a signal sequence that is cleaved, presumably by a signal peptidase, during export to the periplasm, and the periplasmic STb is then translocated to the extracellular medium (Kupersztoch et al., 1990). We have demonstrated that export of STb to the periplasm requires both SecA and electrochemi-

Reprint requests to: Lila M. Gierasch, Department of Chemistry, University of Massachusetts, Amherst, Massachusetts 01003; e-mail: gierasch@chem.umass.edu.

Abbreviations: 2D, 3D, two-, three-dimensional; CAPS, 3-(cyclohexylamino)-propanesulfonic acid; CD, circular dichroism; DTT, dithiothreitol; FID, free induction decay; FPLC, fast protein liquid chromatography; HMQC, heteronuclear multiple quantum coherence; HSQC, heteronuclear single quantum coherence; NMR, nuclear magnetic resonance; NOESY, nuclear Overhauser enhancement spectroscopy; RMSD, RMS deviation; TFA, trifluoroacetic acid; TMSP, 3-(trimethylsilyl)propionic acid; TOCSY, total correlation spectroscopy; Tris, tris(hydroxymethyl)aminomethane.

cal potential (Kupersztoch et al., 1990). STa interacts with an enterocyte receptor that activates guanylate cyclase, which, in turn, leads to an increased intestinal secretion (Field et al., 1978; Guérrant et al., 1980). Recently, it has been reported that intestinal particulate guanylate cyclase serves as an STa receptor (Schulz et al., 1990). In contrast to STa, very little is known about the mechanism of action of STb. The receptor for STb has not been identified, and, unlike STa, STb does not cause a cyclic nucleotide response in the gut. We have recently suggested that STb opens a G-protein-linked receptor-operated Ca^{2+} channel in the plasma membrane (Dreyfus et al., 1993), and that STb causes a dose-dependent release of 5-hydroxytryptamine and prostaglandin E_2 in the gut of treated rats (Harville & Dreyfus, 1995).

The disulfide bridges in STb have been identified by tryptic peptide analysis and Edman degradation to be between Cys 10 and Cys 48 and between Cys 21 and Cys 36 (Dreyfus et al., 1992). Figure 1 shows the primary sequence of STb. Disulfide bridges appear to play a central role in stabilizing the toxin against proteolytic cleavage in the periplasm and also in determining the biological activity of the extracellular STb. There is evidence to suggest that disulfide bond formation is a periplasmic event (Kupersztoch et al., 1990). Mutants that lack disulfides are more susceptible to periplasmic proteolysis than is wild-type toxin (Dreyfus et al., 1992). Disulfides are also important for activity; reduction and *S*-carboxyamidomethylation result in loss of toxicity (Dreyfus et al., 1992).

The loop formed by Cys 21 and Cys 36 contains four glycine residues and has several charged residues. The contribution of some residues in the loop to the toxicity of STb has been examined by site-directed mutagenesis (Dreyfus et al., 1992). The activity of the mutants was determined by directly measuring the volume of the fluid accumulated in ligated rat intestinal loops following STb injection (Whipp, 1990). Among the three mutant peptides that were competent to translocate through the *E. coli* inner and outer membranes, the activity of mutant L26I was indistinguishable from that of the wild-type peptide. In contrast, R29S had ~10% of the activity of the wild-type peptide, and D30V had ~40% of wild-type activity, suggesting that R29 and D30 are among the residues important for toxicity. The mutants R29S and D30V could not compete with native STb, suggesting that these mutant peptides do not efficiently bind the putative receptor (Dreyfus et al., 1992). Recent evidence suggests that the positive residues K22 and K23 are also very important for toxic activity (Fujii et al., 1994).

We have determined the solution structure of STb in an attempt to understand the mechanism of secretion and the toxic activity of STb (see Kinemage 1). The structure of STb would also be useful in the design of appropriate fusion proteins to improve the antigenicity of the peptide, in attempts to develop STb-based vaccines, and also in the design of drugs that inhibit the toxic activity of STb. In addition, STb has two disulfide bridges that are crucial for biological activity, and the structure of STb would provide an opportunity to examine the importance of these in stabilizing the structure. The structure was examined by 2D and 3D NMR methods and CD spectroscopy. A set of approximate interproton distances derived from an analysis of NOEs along with the two disulfide covalent constraints was used to generate structures of STb using distance geometry and simulated annealing. The effect of reducing the disulfides on the structure of STb was examined by CD spectroscopy. The cooperativity of disulfide bond formation and the role of secondary structure inherent to STb in stabilizing the disulfide bonds were investigated by chromatographic analysis of equilibrium mixtures of STb in redox buffers containing oxidized and reduced DTT.

Results and discussion

Experimental conditions for NMR experiments

Initial experiments were aimed at determining the appropriate pH and temperature for NMR experiments. CD experiments suggested that the secondary structure of STb is fairly independent of pH between 4.0 and 11.0. A pH of 4.0 was chosen for NMR experiments in order to keep the saturation of amide resonances due to water suppression to a minimum. Preliminary 2D NMR experiments suggested that the best data could be obtained at 15 °C.

Initially, 3D NOESY-HMQC and 3D TOCSY-HMQC data were collected in water at pH 4.0 and 15 °C. Under these conditions, although data for most of the residues were of good quality, several of the residues in the C-terminal half of the molecule showed broad peaks in the ^1H-^{15}N HSQC spectra (Fig. 2A), which resulted in a poor signal-to-noise ratio in the 3D data sets. A preliminary structural model built based on these data suggested that the molecule exposes hydrophobic residues (in the region 35–45) to the solvent, which might result in aggregation. We reasoned that such an aggregation might result in exchange broadening. We therefore examined the effect of adding meth-

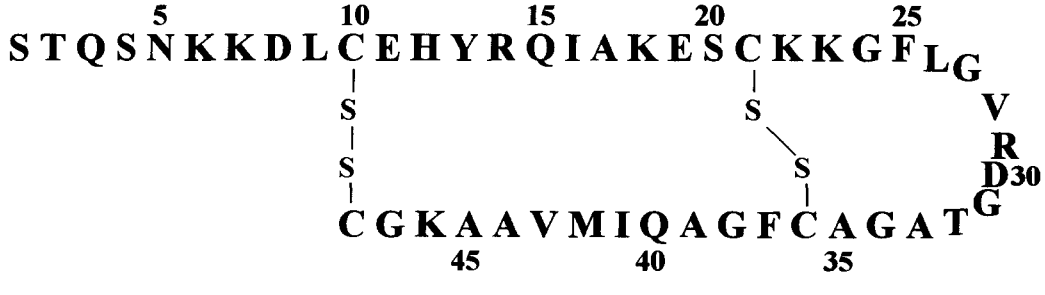

Fig. 1. Amino acid sequence of STb. Disulfide bonds are indicated. Numbering of residues refers to the mature protein, after the cleavage of the presequence.

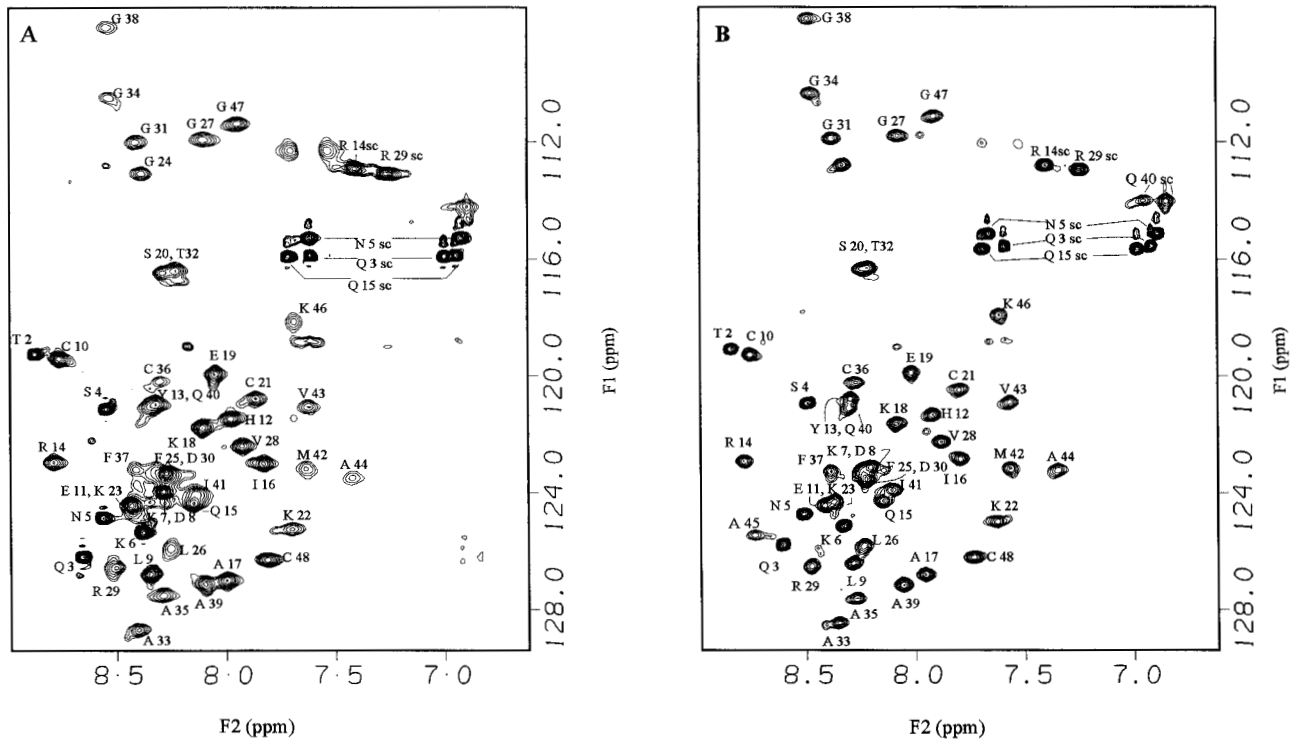

Fig. 2. ^{1}H-^{15}N HSQC spectra of STb at pH 4.0 and 15 °C in water (**A**) and in the presence of 13% CD_3OD (**B**) under the same conditions. Assignment of the cross peaks to individual amide groups is indicated. Notice considerable sharpening of several cross peaks in B.

anol to the STb sample on the HSQC spectra. Addition of increasing amounts of methanol progressively sharpened several cross peaks. Figure 2 compares the HSQC spectra of STb in water (Fig. 2A) and 13% (v/v) methanol (Fig. 2B) at 15 °C. The cross peaks are considerably sharper in 13% methanol and have a better signal-to-noise ratio. It is interesting to note that the broadening in water is rather selective, suggesting that it might also be due to an intramolecular conformational exchange, with methanol making the process faster, driving it from the fast side of the intermediate exchange to fast exchange. Comparison of CD spectra in water and 13% methanol at pH 4 showed that they are virtually superimposable. In addition, the HSQC spectra under these two conditions are very similar and no significant differences were observed in the NOE data, except for the observation of additional cross peaks involving the sharpened amide resonances in the data obtained with 13% methanol. Thus, the structure of STb is not affected by the addition of 13% methanol and we used the data acquired in this solvent system for structure determination.

Resonance assignments

Resonance assignments were obtained by first identifying the spin systems characteristic of different amino acids, using 2D TOCSY and 3D TOCSY-HMQC data. All the NOEs to a particular amide proton were compiled by analyzing the 2D ($\omega 1$, $\omega 3$) planes at the corresponding ^{15}N chemical shift ($\omega 2$). Sequential αN (i, $i+1$), βN (i, $i+1$), and NN (i, $i+1$) NOEs were then used to arrive at sequence-specific assignments. The individual planes were then arranged according to the amino acid sequence as the assignment progressed. Sequential amide–amide NOEs could be observed for most of the molecule, facilitating assignments. Table 1 lists the chemical shifts for STb in water at pH 4.0 and 15 °C. Unambiguous assignments for some of the side-chain protons could not be obtained by this procedure. Figure 3 shows composites of 2D ($\omega 1$, $\omega 3$) planes from 3D ^{1}H-^{15}N NOESY-HMQC spectra corresponding to the N-terminal helix (residues 5–23).

Secondary structure

Figure 4 summarizes the sequential and medium-range NOEs observed in the 3D NOESY-HMQC and 2D NOESY spectra. Also shown in Figure 4 is the α-proton chemical shift index, which allows correlations to be made between the chemical shift and the secondary structure (Wishart et al., 1992). Both the sequential amide–amide NOEs and the medium-range $\alpha\beta$ (i, $i+3$) NOEs qualitatively suggest that the molecule is helical between residues 6 and 23 and 35 and 46. This is consistent with the α-proton chemical shifts. With a few exceptions, the Hα chemical shifts of residues 6–23 and 34–47 are shifted upfield relative to their random-coil values. In contrast, Hα chemical shifts of several of the residues in the loop region (residues 24–34) are close to the random-coil values.

We also carried out deuterium exchange experiments at pD 4.0 and 15 °C, in order to evaluate the protection of amide protons. The deuterium exchange was monitored by measuring HSQC spectra of the sample in D_2O as a function of time. In the earliest HSQC spectrum that could be recorded, ~20 min after dissolution, only the cross peaks corresponding to residues 13–20,

Table 1. *^1H and ^{15}N chemical shifts of STb in aqueous methanol (13/87, v/v), at pH 4.0 and 15 °C*

Residue	N	H^N	H^α	H^β	Other
Ser 1				4.29	4.09
Thr 2	120.03	8.82	4.30	4.10	H^γ, 1.21
Gln 3	127.32	8.59	4.30	1.99, 2.07	H^γ, 2.36; H^δ, 6.92, 7.59; N^δ, 115.55
Ser 4	122.06	8.48	4.32	3.80, 3.89	
Asn 5	126.11	8.49	4.69	2.86, 2.70	H^δ, 6.96, 7.67; N^δ, 115.65
Lys 6	126.51	8.32	4.12	1.85	H^γ, 1.46; H^δ, 1.70; H^ϵ, 2.87
Lys 7	124.89	8.19	4.08	1.85	H^γ, 1.46; H^δ, 1.64; H^ϵ, 2.86
Asp 8	124.89	8.18	4.43	2.69	
Leu 9	128.13	8.27	4.08	1.77	H^γ, 1.62; H^δ, 0.86
Cys 10	120.44	8.74	4.80	2.97, 3.12	
Glu 11	125.70	8.41	4.09	2.15	H^γ, 2.41
His 12	122.46	7.90	4.42	3.20, 3.37	2H, 8.39; 4H, 7.14
Tyr 13	122.06	8.28	4.17	2.95, 3.12	H^δ, 7.15; H^ϵ, 6.81
Arg 14	124.49	8.77	3.93	1.83, 1.96	H^γ, 1.56; H^δ, 3.09, 3.21; NH, 7.39
Gln 15	125.70	8.14	4.00	2.15–2.22	H^γ, 2.41; H^δ, 6.86, 7.65; N^δ, 115.10
Ile 16	124.49	7.78	3.71	1.83	H^γ (CH2), 1.35; H^γ (CH3), 0.82; H^δ, 0.56
Ala 17	128.54	7.94	3.95	1.32	
Lys 18	122.87	8.07	3.87	1.87	H^γ, 1.32,1.49; H^δ, 1.64; H^ϵ, 2.91
Glu 19	121.25	8.01	4.03	2.06	H^γ, 2.42
Ser 20	117.60	8.24	4.25	3.70, 3.86	
Cys 21	121.65	7.79	4.68	2.97, 3.19	
Lys 22	126.51	7.59	4.21	1.83	H^γ, 1.44; H^δ, 1.62
Lys 23	125.30	8.35	4.22	1.80	H^γ, 1.46; H^δ, 1.64; H^ϵ, 2.98
Gly 24	113.96	8.31	3.77, 3.95		
Phe 25	124.89	8.22	4.57	3.08	H^δ, 7.22
Leu 26	127.32	8.22	4.23	1.59	H^γ, 1.48; H^δ, 0.82
Gly 27	113.15	8.06	3.89		
Val 28	123.68	7.86	4.04	2.07	H^γ, 0.89
Arg 29	127.73	8.45	4.27	1.72, 1.82	H^γ, 1.57; H^δ, 3.12; NH, 7.22
Asp 30	124.89	8.21	4.60	2.73	
Gly 31	112.74	8.36	3.98		
Thr 32	117.96	8.20	4.32	4.27	H^γ, 1.15
Ala 33	130.16	8.34	4.17	1.32	
Gly 34	111.53	8.46	3.92		
Ala 35	128.94	8.25	4.20	1.47	
Cys 36	121.65	8.25	4.23	2.94, 3.20	
Phe 37	124.89	8.37	4.25	2.98, 3.10	H^δ, 7.16
Gly 38	109.10	8.48	3.63, 3.88		
Ala 39	128.54	8.04	4.16	1.49	
Gln 40	122.06	8.28	3.94	2.18, 2.29	H^γ, 2.58; H^δ, 6.82, 6.91; N^δ, 114.00
Ile 41	125.70	8.09	3.65	1.81	H^γ (CH2), 0.91, 1.25; H^γ (CH3), 0.72; H^δ, 0.54
Met 42	124.49	7.55	4.09	1.95, 2.28	H^γ, 2.57
Val 43	122.06	7.55	3.93	2.09	H^γ, 0.80, 0.91
Ala 44	124.49	7.32	4.21	1.39	
Ala 45	126.92	8.73	4.02	1.38	
Lys 46	119.22	7.59	4.23	1.86	H^γ, 1.38; H^δ, 1.73
Gly 47	112.34	7.89	3.87–3.97		
Cys 48	127.73	7.71	4.58	2.87, 3.19	

39–46, and 48 could be detected. These cross peaks were still detectable after 11 h of exchange. This exchange behavior is consistent with the assignment of helical structure to these residues.

Distance-geometry calculations

Distance-geometry calculations provide a means of generating conformations that are consistent with NMR-derived distance restraints, starting from randomized coordinates (Havel et al., 1983; Crippen & Havel, 1988; Kuntz et al., 1989; Havel, 1991). These structures, after they are refined to bring the structures into agreement with the distance restraints, represent the range of conformations compatible with the NMR data. A total of 390 distance restraints derived from the NOE data, of which 144 were intraresidue, 133 sequential, 99 medium-range (i, $i+2$, 54; i, $i+3$, 38; i, $i+4$, 7), and 14 long-range, were incorporated into calculations as upper bounds on corresponding interproton distances. Additional NOEs were present but could not be assigned unambiguously because of the degeneracy of the ^1H chemical shifts. An attempt was made to assign additional NOEs

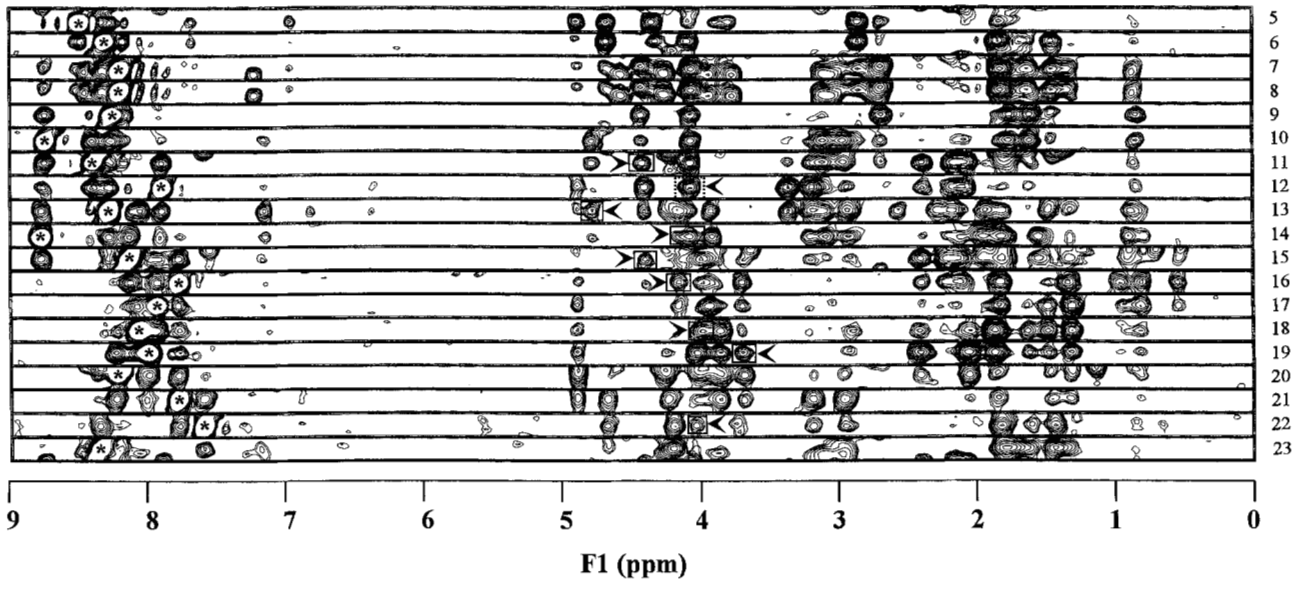

Fig. 3. 2D ($\omega 1$, $\omega 3$) strips from the 3D NOESY-HMQC spectrum of STb, arranged according to the amino acid sequence. Representative data for residues 5–23 are shown. Data were obtained in 13% aqueous methanol at pH 4 and 15 °C with a mixing time of 150 ms. Individual strips are centered (±0.06 ppm) around the chemical shift of the amide proton in $\omega 3$ dimension. In the amide region, the diagonal peaks are shown with only a few outer contours and an asterisk in the center in order to facilitate recognition of sequential amide–amide NOEs. In the H^{α} region, the cross peaks corresponding to αN (i, $i+3$) are boxed and identified with an arrowhead. Dashed box indicates overlap of this medium-range NOE with a sequential NOE.

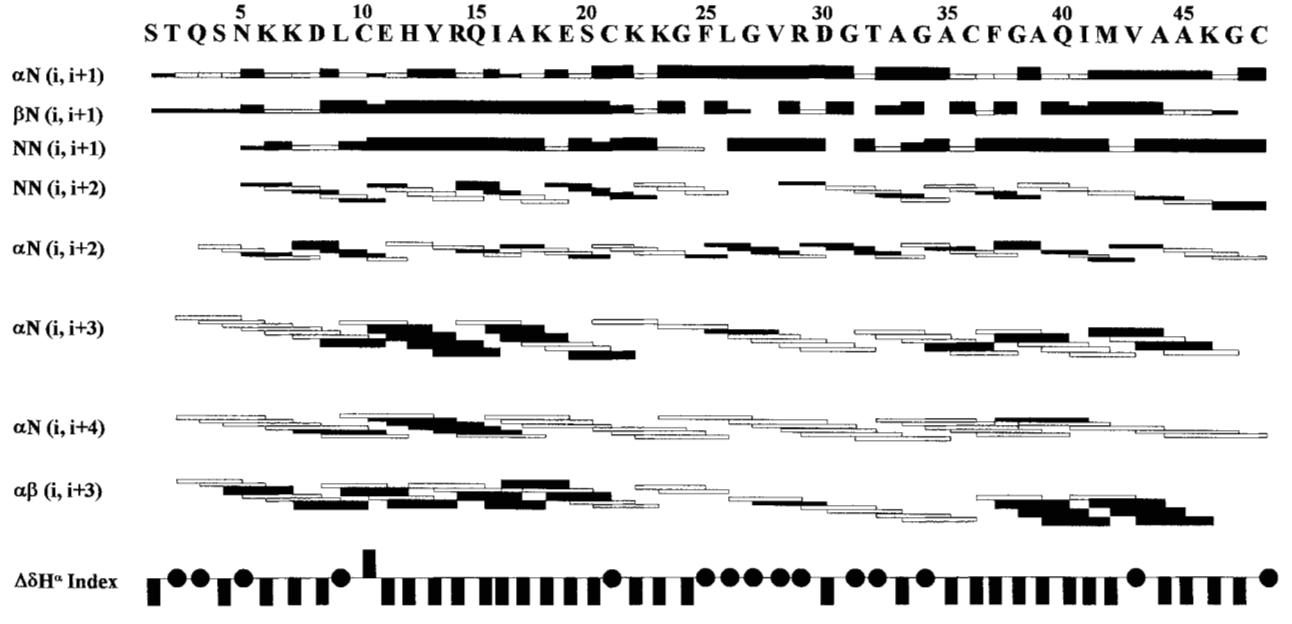

Fig. 4. Summary of sequential and medium-range ($|i-j| \leq 4$) NOEs observed in the 3D NOESY-HMQC and 2D NOESY spectra of STb. Filled bars indicate the observed NOEs; the thickness of the bars reflects the intensity of the NOEs, which are classified as weak, medium, and strong. The intensities were measured by counting the number of contours and normalizing them relative to the number of contours observed for the corresponding amide group in the ^{1}H-^{15}N HSQC spectrum. Unfilled bar indicates an NOE that might be present, but where unambiguous assignment was not possible due to resonance overlap. A blank space indicates that the NOE was absent. $\alpha\beta$ (i, $i+3$) NOEs were observed in the 2D NOESY spectrum under the same conditions. The Wishart index ($\Delta\delta H\alpha$ index) is indicated at the bottom of the figure. A downward bar indicates an H^{α} resonance upfield shifted relative to the random-coil value for that residue; an upward bar indicates a downfield-shifted resonance; a circle indicates an H^{α} chemical shift within the range for a random coil.

after the structure determination, but this was not fruitful due to the fact that ambiguities involved residues in the loop (residues 21–36) whose orientation relative to the rest of the molecule is not well defined in the structure. Details of the distance-geometry procedure are described in the Materials and methods. A total of 20 distance-geometry structures were generated. Two of the distance-geometry structures had relatively high error function values compared to the rest and were discarded from further analysis. The remaining structures were analyzed for their violations from the input distance restraints and similarity of their backbone conformations. These structures satisfy the input distance restraints reasonably well. Most of the violations were <0.1 Å, with a few in the range 0.1–0.7 Å. The average violations for the individual distance-geometry structures ranged from 0.07 ± 0.11 to 0.07 ± 0.13 Å. An analysis of the RMSDs showed that the backbone conformation converged to different extents in different parts of the molecule, and the extent of convergence correlated with the number of restraints in a given region. For example, when residues 5–48 of the distance-geometry structures were superimposed on the average structure, the average RMSDs were 2.5 ± 0.8 Å for superimposing backbone atoms and 3.0 ± 0.74 Å for superimposing all heavy atoms. If the loop region, residues 21–36, is excluded from superposition, the average RMS values drop substantially to 1.27 ± 0.29 Å and 1.93 ± 0.44 Å for backbone and heavy atoms superpositions, respectively. Thus, the loop region from residues 21 to 36 converges poorly, relative to the rest of the molecule. The average RMSDs for this region of the molecule considered separately are 2.6 ± 0.24 Å and 3.5 ± 0.32 Å for backbone and heavy atom superpositions, respectively. Also, the orientation of the loop region 21–36 relative to the rest of the molecule converges poorly, due to the absence of NOEs between these two parts of the molecule. Figure 5 shows a superimposition of the Cα trace of all the distance-geometry structures. This overlay was obtained by superimposing backbone atoms of residues 3–21 and 36–48 as one structural unit and those of the loop region (residues 21–36) separately. It is evident from this superposition that backbone conformation for residues 5–22 and 35–46 converges reasonably well. Two alternate conformations appear to be equally compatible with the NOE data around residue 47.

One of the distance-geometry structures, that with the lowest error function value, was further refined by restrained energy minimization. The details of the procedure are described in the Materials and methods. Figure 6 and Kinemage 1 show the resulting structure. A variable width ribbon, which reflects the relative average RMSDs at each residue, is superimposed on the structure. These average RMSDs are derived from the superposition of distance-geometry structures shown in Figure 5. In this structure, the backbone ϕ,ψ dihedral angles of all residues, with the exception of Leu 9 and Thr 32, are within the allowed regions of the Ramachandran map (Ramachandran & Sasisekharan, 1968). We have carefully examined the NOE assignments involving these residues for possible spin-diffusion effects and did not find any. The deviation of L9 and T32 is presumably a result of energy minimization in the absence of solvent and/or due to a conflict between multiple pseudo-force constants representing the distance restraints. These distortions are relieved when energy minimization was carried out in the absence of restraints. This yielded a structure with a very similar backbone conformation but, as expected, this structure shows larger violations from the input distance restraints. Both of these minimized structures share the structural features described below.

The structure shows two helical regions, one from residues 10 to 22 and the other from residues 38 to 44. The backbone dihedral angles in these regions are more distorted from the ideal helical values in the structure shown in Figure 6 and Kinemage 1 but are closer to the ideal values in the structure minimized without restraints. The N-terminal helix is amphipathic, with the side

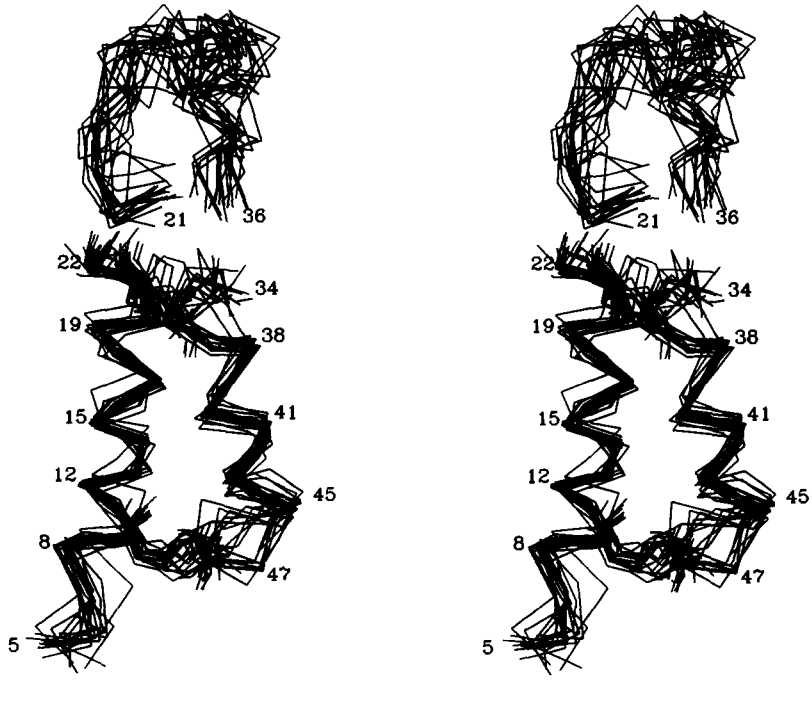

Fig. 5. Stereo diagram of superposition of 18 of 20 distance-geometry structures calculated using the NOE data. Backbone atoms of residues 5–23 and 34–48 are superimposed as one structural unit. Backbone atoms of residues 21–36 are superimposed separately. Only C^{α} atoms are shown for clarity. Heavy atoms of Cys residues are also shown. Selected residues are labeled.

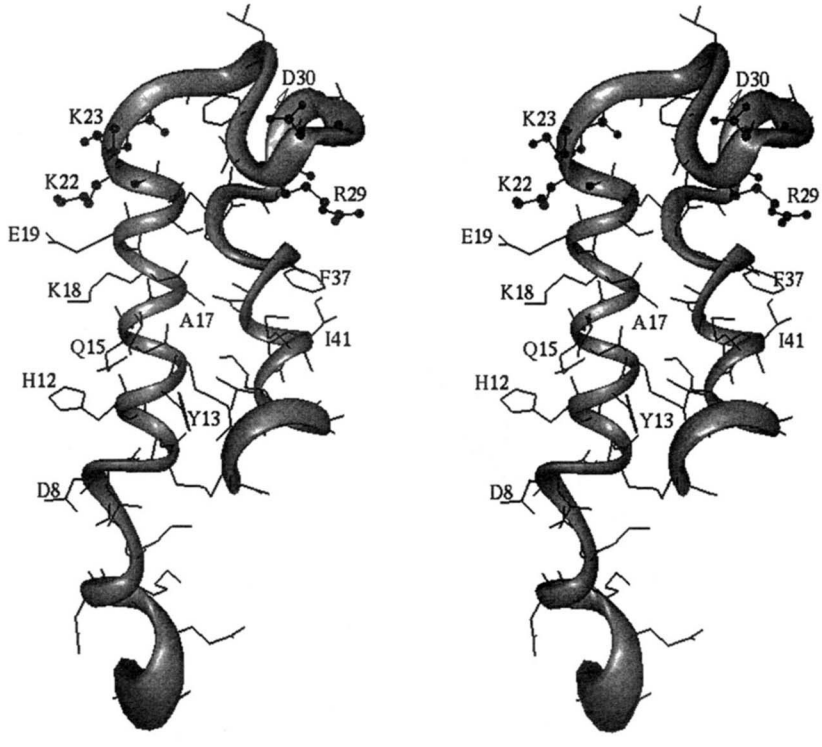

Fig. 6. Stereo diagram of energy minimized structure of one of the distance-geometry structures, with least-error function. Heavy atoms are shown. A variable width ribbon that reflects the average RMSD at every residue (for the superposition of distance-geometry structures shown in Fig. 5) is shown. The average RMSDs ranged from 0.9 to 3.5 Å for residues 3–48 and were 5.7 Å and 8.8 Å for residues 1 and 2, respectively. Selective residues are labeled. Side chains of residues that have been shown to be important for toxicity are given as ball and stick representations.

chains of Asp 8, His 12, Gln 15, Lys 18, Glu 19, Lys 22, and Lys 23 pointing into the solvent, making a highly polar surface. It is interesting to note that Lys 22 and Lys 23 have been shown to be important for toxic activity (Fujii et al., 1994). The role of other charged residues in this region of the molecule in determining the toxic activity has not yet been explored. Several hydrophobic residues from the opposite face of the N-terminal helix are in contact with the hydrophobic residues from the C-terminal helix. For example, Tyr 13 and Arg 14 extend their side chains into the hydrophobic interior of the molecule and make contacts with Val 43, whereas Ala 17 side chain is in contact with Ala 39 and Gln 40 side chains. The helices pack rather loosely, leaving a gap of subatomic dimensions between these two clusters.

The C-terminal helix is relatively more hydrophobic; Ile 41, Met 42, and Phe 37 form a hydrophobic cluster, and Ile 41 also makes contact with the side chain of R29 in the loop region. The loop region (residues 21–36), linked by the disulfide bond, may be defined as an Ω loop (Leszczynski & Rose, 1986). This region is devoid of regular secondary structure, with the exception of a type III′ β-turn centered around residues 35 and 36. The C^{α}–C^{α} distance between the ends of the loop is short (4.7 Å) and the loop forms a well-packed structure by itself. Residues Phe 25, Val 28, Ala 33, and Ala 35 in the loop region form a hydrophobic cluster, while exposing the charged residues Arg 29 and Asp 30 to the solvent. We have previously shown that mutation of either of these charged residues significantly affects the toxic activity of STb (Dreyfus et al., 1992).

The chirality of the disulfide could not be deduced from the NOE data due to overlap of Cys Hβ resonances. The CD spectrum of STb in the near UV region (Fig. 7) enables estimates of the magnitude of the dihedral angle around the S–S bond to be made. At pH 6.5, the CD spectrum in the near UV region shows a single negative band around 270 nm. Because this region of the CD spectrum could have overlapping contributions from the tyrosyl side chain, the pH of the sample was increased to 11 in order to ionize the tyrosyl side chain and thus shift the tyrosine

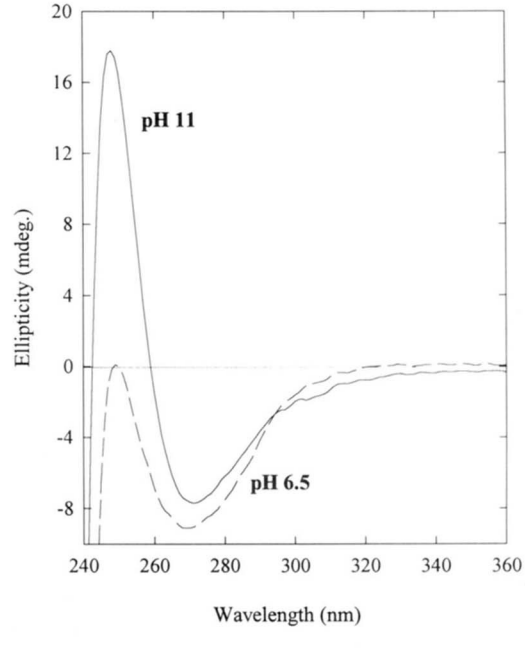

Fig. 7. Near-UV CD spectrum of STb showing disulfide bond contributions at pH 6.5 and pH 11. Five-millimeter pathlength cells were used at a protein concentration of 50 μM, in 5 mM KPi, pH 6.5 (— —) or 5 mM CAPS, pH 11.0 (——).

contribution to a higher wavelength. This reveals a positive band at 248 nm. At this pH, the negative band around 270 nm is retained. Although it is difficult to delineate the contributions of the two disulfide bonds to these two bands, the strong CD band at 248 nm suggests that a significant population of the rotamers have S-S dihedral angles close to ±90°. The long wavelength band at 270 nm suggests a contribution from rotamers with dihedral angles deviating by ~30° from 90° (Boyd, 1972; Donzel et al., 1972). This estimate is consistent with the dihedral angles observed in the distance-geometry structures.

Role of disulfide bonds in stabilizing the structure of STb

The disulfide bonds in STb have been shown to be crucial for its toxic activity (Dreyfus et al., 1992; Y. Arriaga, B.A. Harville, and L.A. Dreyfus, unpubl. results). We examined the effect of reducing the disulfide bonds on the secondary structure of STb by CD spectroscopy. STb was reduced by incubating in 10 mM DTT at 37 °C and the reduction was followed by testing aliquots on reverse-phase HPLC. After the reduction was judged complete by HPLC, the CD spectrum of the reduced form was recorded after appropriate dilution. Figure 8 shows the CD spectra of native and reduced STb at pH 7 and 10 °C. It is evident that reduction is accompanied by dramatic loss of structure. Estimation of secondary structure for each of these spectra by CONTIN (Provencher & Glöckner, 1981; Provencher, 1982) indicated that native STb has about 73 ± 2% helix and 4 ± 2% β-structure, and 22% remainder, whereas reduced STb is composed of 20% helix, 29% β-structure, and 51% remainder. Thus, the disulfide bonds stabilize the native structure of STb.

Cooperativity of disulfide bond formation and the role of secondary structure in stabilizing the disulfide bonds

The CD studies discussed above have shown that disulfide bonds are important in stabilizing the native secondary structure. We wanted to investigate the importance of secondary structure on the stabilities of disulfides and also examine if the formation of two disulfide bonds is cooperative, by measuring the equilibrium populations of native, fully reduced, and single-disulfide intermediates in equilibrium mixtures of STb in DTT redox buffers. Similar studies on apamin, an 18-residue peptide containing two disulfide bonds, have shown that disulfide bond formation in this peptide is very cooperative and that the native disulfides are only moderately stabilized by urea denaturable secondary structure (Chau & Nelson, 1992). Figure 9A shows the HPLC chromatogram of an equilibrium mixture of STb in 1:100 DTT: DTT-oxidized. The peaks due to the native and reduced STb were identified by analyzing STb under fully oxidizing or reducing conditions, respectively. In Figure 9A, in addition to the native and fully reduced species, significant concentrations of single-disulfide intermediates could be detected, which suggests that the disulfide bond formation in STb is only moderately cooperative. For STb, with four Cys residues, six single-disulfide intermediates and two two-disulfide species (in addition to the native form) are possible. At least seven of these species could be detected in the equilibrium mixture; some of these were overlapped in the HPLC chromatogram and could not be resolved further. Although unambiguous assignment of these peaks to the individual species is difficult, two well-resolved peaks marked SD are at higher concentrations relative to the others. If these are assigned to single-disulfide intermediates with native-like disulfides, we obtain an equilibrium constant of $\sim 4 \times 10^{-3}$ for the formation of a single-disulfide intermediate from the reduced form and an equilibrium constant of $\sim 7 \times 10^{-2}$ for the formation of the second disulfide bond, based on the integration of peak areas. This represents an 18-fold increase over the formation of the first disulfide, which is quite moderate compared to the cooperativity observed in apamin where the formation of the second disulfide has an equilibrium constant that represents a 680-fold increase over the first one (Chau & Nelson, 1992). This suggests that in STb the formation of the first disulfide bond does not constrain the molecule as much as it does in apamin, to favor the formation of the second disulfide.

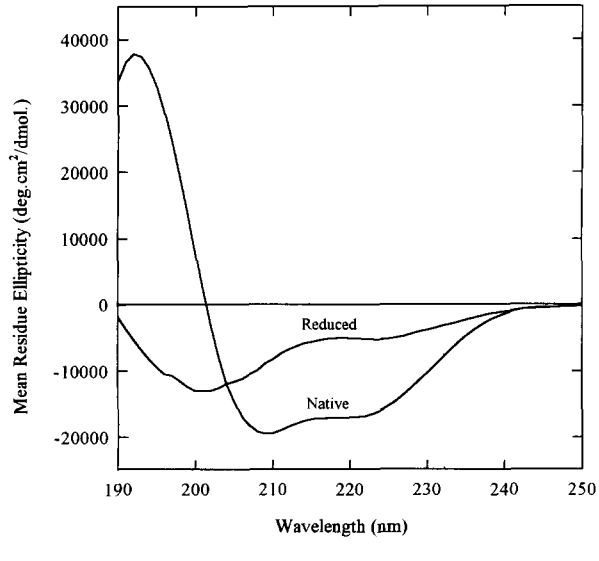

Fig. 8. CD spectra of native and reduced STb at pH 7. Protein concentration was ~7 μM. Data collected every nanometer for 3 s were averaged over three scans, baseline subtracted, and smoothed.

In order to evaluate the role of urea denaturable secondary structure in determining the stabilities of the native disulfides, a similar experiment was carried out in the presence of 8 M urea. Figure 9B shows the chromatogram. The relative concentrations of reduced and native species change dramatically in the presence of urea. Integration of peak areas shows that the equilibrium constant for the formation of native from fully reduced STb decreases by a factor of ~40 in the presence of urea. On the other hand, the equilibrium constant for the formation of single-disulfide intermediate from reduced decreases only by a factor of 5–10. Thus, it appears that the helical structure plays a greater role in stabilizing the two disulfide bonds simultaneously and is less crucial for maintaining any one of the disulfides.

The results presented here show that STb is a predominantly helical molecule, and the helical structure is significantly stabilized by the disulfide bonds. Several of the residues in the loop region between residues 21 and 36 have been shown to be important for toxic activity. The importance of other residues in the helical structural unit, stabilized by disulfide bonds or the N-terminal nine amino acids, remains to be explored. The mobility of the loop region observed in the present study may be of functional significance. It will be of interest to examine if a peptide corresponding to the loop region 21–36, incorporating

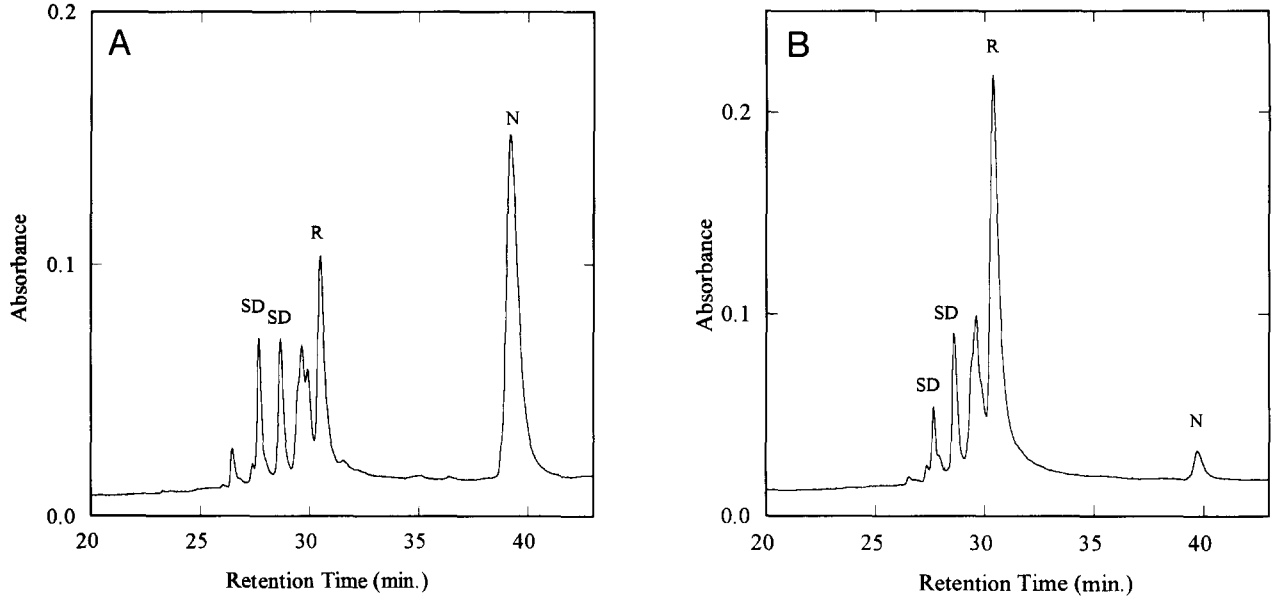

Fig. 9. HPLC traces of equilibrium mixtures of STb in a DTT redox mixture in the absence (**A**) and in the presence (**B**) of 8 M urea. N and R refer to native and reduced STb, respectively. Peaks that are tentatively assigned to single-disulfide intermediates, with native-like disulfides, are labeled SD. See text for details of experimental procedures.

the disulfide bond between 21 and 36, is sufficient for toxicity. These studies are currently underway.

Neither the amino acid sequence nor the disulfide bonding pattern of STb shares any similarities with other peptide or protein toxins containing disulfides. The 3D structures of several of these toxins have been determined, for example, antimicrobial defensins (Pardi et al., 1992), the scorpion toxins iberiotoxin (Johnson & Sugg, 1992), P05-NH2 (Meunier et al., 1993), spider toxin ω-Aga IV B (Yu et al., 1993b), the toxin-agglutinin Hevein (Andersen et al., 1993), the snake venom toxins sarafotoxin SRTb (Atkins et al., 1995), fasciculin (Le Du et al., 1992), cardiotoxin VII4 (Rees et al., 1990), bungarotoxin (Oswald et al., 1991), cardiotoxin (Gilquin et al., 1993), cobrotoxin II (Yu et al., 1993a), sea anemone toxin ATX IA (Widmer et al., 1989), bee venom toxin, tertiapin (Xu & Nelson, 1993), and snail toxin ω-conotoxin (Davis et al., 1993). None of these structures resembles the structure of STb determined here. The central structural motif in STb, two disulfide bonds linking two helices, is relatively rare in protein structures. We found only three examples of a disulfide linking two helices in the Protein Data Bank (Bernstein et al., 1977; Abola et al., 1987); one of the disulfide bonds in crambin (Teeter, 1984) and in glutathione reductase (Karplus & Schulz, 1987) links two short helices. In phospholipase A2, two disulfides link two long helices that are perfectly antiparallel (Dijkstra et al., 1981).

Materials and methods

STb preparation

STb was purified by a modification of a previously reported method (Dreyfus et al., 1992). Briefly, *E. coli* 1790 (Shannon C. Whipp, U.S. Department of Agriculture, Agricultural Research Services, National Animal Disease Center, Ames, Iowa) harboring pPD21K (Urban et al., 1990), a kanamycin-resistant derivative of plasmid pPD21, used as a source of the STb gene, was grown at 37 °C with vigorous aeration in 24 L of M9 medium (Maniatis et al., 1982) containing 0.2% glucose and kanamycin (50 μg/mL). After 18 h of growth, the bacterial cells were removed by filtration at room temperature through a 0.1-μm hollow fiber cartridge attached to an Amicon DC-10 preparative ultrafiltration device. High molecular weight material was removed from the filtrate by passage through a 100-kDa exclusion spiral membrane cartridge. The filtrate was concentrated over a 3-kDa exclusion spiral membrane cartridge to a final volume of approximately 1 L. The concentrated filtrate was then pumped at a flow rate of 30 mL/min onto a DeltaPak C4 RCM preparative (25 mm × 100 mm) HPLC column. Bound material was eluted from the column with a step gradient of methanol containing 0.05% TFA. The eluate was monitored at 220 nm. STb eluted at 60% methanol. Methanol was evaporated, and the solvent was exchanged over a Fast Desalt column (Pharmacia, Piscataway, New Jersey) equilibrated in 0.05 M sodium phosphate buffer (pH 6.5). The sample was then fractionated by cation-exchange FPLC on a mono-S column equilibrated in the same buffer. Material that bound to the mono-S column was eluted with a linear gradient of NaCl (0–1.0 M) in phosphate buffer, pH 6.5. STb eluted as a single peak at approximately 0.3 M NaCl. Aliquots of the STb-containing peak were analyzed for purity by reverse-phase FPLC on a PepRPC 15 column (Pharmacia, Piscataway, New Jersey) equilibrated in water containing 0.05% TFA and developed with a linear gradient of 0–100% acetonitrile containing 0.05% TFA. Pure STb eluted as a single sharp peak at approximately 60% acetonitrile. The material was further analyzed by SDS-PAGE (12.5% T, 6% C) in tricine buffer (Schagger & von Jagow, 1987) and automated Edman degradation using a model 470 automated sequencer (Applied Biosystems, Foster City, California).

^{15}N-labeled STb was prepared in the same manner as unlabeled STb with the exception that $^{15}NH_4Cl$ (^{15}N, 97%; Cambridge Isotope Laboratories, Andover, Massachusetts) was the sole source of nitrogen in the M9-glucose medium.

CD

CD spectra were recorded on an Aviv model 62DS spectrometer, using cells of 1-mm pathlength. The temperature was regulated by a built-in thermoelectric holder. Peptide concentrations were ~7 μM in 5 mM citrate (pH 4–5), phosphate (pH 6–7), Tris (pH 8–9), or CAPS (pH 10–11) buffer. Higher peptide concentrations and 5-mm pathlength cells were used for recording the CD signal in the near-UV region (240–300 nm). Data collected every nanometer for 3 s were averaged over three scans, baseline subtracted, and smoothed. Estimates of secondary structure were obtained using the program CONTIN (Provencher & Glöckner, 1981; Provencher, 1982).

NMR spectroscopy

All the NMR data were acquired on a Varian VXR500 spectrometer operating at a ^{1}H frequency of 500 MHz. All the data were obtained at 15 °C on 1.5–2.0 mM samples in 90% H_2O/10% D_2O or 87% H_2O/13% CD_3OD at pH 4.0, in a total sample volume of 0.7 mL. Samples uniformly labeled with ^{15}N were used for 2D HSQC, 3D NOESY-HMQC, and 3D TOCSY-HMQC experiments. Both labeled and unlabeled samples were used for 2D NOESY and 2D TOCSY experiments. Chemical shifts were measured with respect to TMSP as an internal standard. ^{15}N chemical shifts were measured relative to an external standard (200 mM $^{15}NH_4Cl$ in 1 M HCl referenced at 24.93 ppm). Data processing was done on a Silicon Graphics 4D/25 Personal Iris workstation using the program Felix (Biosym Technologies Inc.). All the spectra were acquired in phase-sensitive mode with quadrature detection (States et al., 1982). A relaxation delay of 1 s was used in all cases. Two-dimensional NOESY (Jeener et al., 1979; Kumar et al., 1981) and TOCSY (Davis & Bax, 1985) spectra were acquired with a spectral width of 6,800 Hz in both dimensions and mixing times of 150 and 60 ms, respectively. The water signal was suppressed by low-power presaturation, and, in the case of ^{15}N-labeled samples, nitrogen was decoupled during ^{1}H evolution and during the acquisition time. A WALTZ17 (Bax, 1989) mixing sequence was used for TOCSY experiments with the introduction of two delays before and after the 180° pulse for the suppression of cross relaxation (CLEAN-TOCSY) (Griesinger et al., 1988). Two × 256 FIDs, each of 768 complex points, were acquired with 64 scans per FID. A zero-order baseline correction was applied after Fourier transformation of the $t2$ dimension, and linear prediction of the first point of each FID was used to obtain flat base planes. Data were apodized using Gaussian or shifted sine-bell functions. Zero filling and Fourier transformation in $t1$ and $t2$ dimensions yielded matrices of 1K × 1K real points.

^{1}H-^{15}N HSQC spectra (Bodenhausen & Ruben, 1980) were recorded with spectral widths of 6,800 Hz in the proton dimension and 1,290 Hz in the nitrogen dimension. A 3-ms spin-lock purge pulse was used to suppress the water signal (Messerle et al., 1989), which was further removed during data processing with a low-frequency filter in the time domain (Marion et al., 1989b). Two × 100 FIDs of 768 complex points with 32 scans per FID were collected and processed as described above to obtain matrices of 512 × 512 real points after discarding all the data upfield to water in the $\omega 2$ dimension.

Three-dimensional ^{1}H-^{15}N TOCSY-HMQC and NOESY-HMQC (Marion et al., 1989a, 1989c; Zuiderweg & Fesik, 1989) data were acquired using pulse sequences adapted for solvent suppression with two spin-lock purge pulses of 0.5 and 2 ms duration (Messerle et al., 1989). The spectral widths along $\omega 3$, $\omega 2$, and $\omega 1$ dimensions were 6,800 Hz, 1,290 Hz, and 5,400 Hz, respectively; 768 complex $t3$, 29 complex $t2$, and 110 complex $t1$ data points were obtained with 16 scans per FID, resulting in a total acquisition time of ~3 days. The mixing times used were 50 and 150 ms for the TOCSY-HMQC and NOESY-HMQC, respectively. A low-frequency filter was applied before data processing (Marion et al., 1989b). The apodization functions used were a Gaussian for the $t3$ domain, a 45° shifted sine bell added to a 100-Hz line-broadening exponential for the $t2$ domain (Fesik & Zuiderweg, 1990), and a 70 degree-shifted sine bell for the $t1$ domain. Zero-order baseline corrections were applied after Fourier transformation along the $t3$ and $t2$ dimensions, and the first point of each FID along the $t2$ and $t1$ domains was calculated by linear prediction. Zero filling and removal of the aliphatic part of the spectrum in the $\omega 3$ dimension yielded matrices consisting of 512 × 64 × 512 real points.

Distance geometry

Distance-geometry calculations were carried out using the program DGII within InsightII (NMRchitect software, Biosym Technologies, San Diego, California) on a Silicon Graphics 4D/25 Personal Iris workstation. The DGII program is based on the EMBED algorithm (Havel et al., 1983; Kuntz et al., 1989; Havel, 1991). The calculation starts with randomized coordinates and involves bound smoothing, embedding, majorization, and optimization using a simulated annealing protocol. The NOEs were classified as strong, medium, weak, or very weak in intensity based on the number of contours in the cross peaks and 2.7, 3.3, 4.0, or 4.5 Å were used as upper bounds for the corresponding interproton distances. The region from residues 10–22 forms a well-defined helix and the NOE intensities in this region of the molecule were used as guidelines for this classification. Methyl and methylene groups were replaced by pseudo atoms at their corresponding centers of mass, and the upper bounds were corrected appropriately, by adding 1 and 1.5 Å, respectively. Distance restraints were incorporated into the calculation in the form of skewed biharmonic potential energy functions, with a force constant of 30 kcal·mol^{-1}·Å^{-2}. A total of 20 distance-geometry structures were calculated and analyzed for convergence of backbone conformation and for their violations from the input distance restraints.

For further refinement of the structure, one of the distance-geometry structures was subjected to restrained energy minimization in the presence of the same set of distance restraints as was used for distance-geometry calculations. A 12-Å cut-off was used for nonbonded interactions. Charge interactions were included and a distance-dependent dielectric, set to 1× internuclear distance, was used. A quartic nonbonded form was used during initial stages of minimization, which was later replaced by a Lennard-Jones potential. A consistent valence force field was used without Morse and cross terms (Dauber-Osguthorpe et al., 1988). Atomic coordinates of the energy-minimized structure (access code 1EHS) and the list of NMR-derived distance

restraints (access code R1EHSMR) have been deposited at the Brookhaven Protein Data Bank.

HPLC analysis of STb in redox buffers

The redox reaction was initiated by dissolving a lyophilized sample of STb in redox buffer – 50 mM potassium phosphate, 0.2 M KCl, and 1 mM EDTA adjusted to pH 8.7, containing 10 mM redox mixture (1:100 DTT:DTT oxidized), predegassed under sonication and kept under nitrogen atmosphere (Creighton, 1986). The final concentration of STb was 25 μM in a total volume of 200 μL. The mixture was left at room temperature under nitrogen. At various intervals, the exchange was quenched by adding 100 μL of 25% TFA and analyzed immediately by HPLC on an analytical reverse-phase C18 column (Vydac), using an acetonitrile-water gradient. Equilibration was generally achieved within 2 h. The gradient was optimized to resolve the maximum number of species. The following gradient was chosen: 10–27% acetonitrile in the first 5 min, 27–35% acetonitrile in the next 17 min, 35–100% acetonitrile in the last 24 min. Solvents contained 0.1% TFA. The absorbance of the eluate was followed at 220 nm.

Supplementary material in the Electronic Appendix

One table of NMR-derived restraints used in the generation of distance-geometry structures is contained in the Electronic Appendix.

Acknowledgments

This research was supported in part by NIH grants GM 27616 (L.M.G.) and AI32736 (L.A.D.).

References

Abola EE, Bernstein FC, Bryant SH, Koetzle TF, Weng J. 1987. Protein Data Bank. In: Allen FH, Bergerhoff G, Sievers R, eds. *Crystallographic databases – Information content, software systems, scientific applications*. Bonn/Cambridge/Chester: Data Commission of the International Union of Crystallography. pp 107–132.

Andersen NH, Cao B, Rodriguezromero A, Arreguin B. 1993. Hevein-NMR assignment and assessment of solution-state folding for the agglutinin-toxin motif. *Biochemistry 32*:1407–1422.

Atkins AR, Martin RC, Smith R. 1995. ^{1}H NMR studies of sarafotoxin SRTb, a nonselective endothelin receptor agonist, and IRL 1620, an ETB receptor-specific agonist. *Biochemistry 34*:2026–2033.

Bax A. 1989. Homonuclear Hartmann-Hahn experiments. *Methods Enzymol 176*:151–168.

Bernstein FC, Koetzle TF, Williams GJB, Meyer EF Jr, Brice MD, Rodgers JR, Kennard O, Shimanouchi T, Tasumi M. 1977. The Protein Data Bank: A computer-based archival file for macromolecular structures. *J Mol Biol 112*:535–542.

Betley MJ, Miller VL, Mekalanos JJ. 1986. Genetics of bacterial enterotoxins. *Annu Rev Microbiol 40*:577–605.

Bodenhausen G, Ruben DJ. 1980. Natural abundance nitrogen-15 NMR by enhanced heteronuclear spectroscopy. *J Magn Reson 69*:185–189.

Boyd DB. 1972. Conformational dependence of the electronic energy levels in disulfides. *J Am Chem Soc 94*:8799–8804.

Burgess MN, Bywater RJ, Cowley CM, Mullan NA, Newsome PM. 1978. Biological evaluation of a methanol-soluble, heat-stable *Escherichia coli* enterotoxin in infant mice, pigs, rabbits, and calves. *Infect Immunol 21*: 526–531.

Chau MH, Nelson JW. 1992. Cooperative disulfide bond formation in apamin. *Biochemistry 31*:4445–4450.

Creighton TE. 1986. Disulfide bonds as probes of protein folding pathways. *Methods Enzymol 131*:83–106.

Crippen GM, Havel TF, eds. 1988. *Distance geometry and molecular conformation*. Taunton, England: Research Studies Press.

Dauber-Osguthorpe P, Roberts VA, Osguthorpe DJ, Wolff J, Genest M, Hagler AT. 1988. Structure and energetics of ligand binding to proteins: *Escherichia coli* dihydrofolate reductase–trimethoprim, a drug-receptor system. *Proteins Struct Funct Genet 4*:31–47.

Davis DG, Bax A. 1985. Assignment of complex ^{1}H NMR spectra via two-dimensional homonuclear Hartmann-Hahn spectroscopy. *J Am Chem Soc 107*:2820–2821.

Davis JH, Bradley EK, Miljanich GP, Nadasdi L, Ramachandran J, Basus VJ. 1993. Solution structure of ω-conotoxin GVIA using 2-D NMR spectroscopy and relaxation matrix analysis. *Biochemistry 32*:7396–7405.

Dijkstra BW, Kalk KH, Hol WGJ, Drenth J. 1981. Structure of bovine pancreatic phospholipase A2 at 1.7 Å resolution. *J Mol Biol 147*:97–123.

Donzel B, Kamber B, Wüthrich K, Schwyzer R. 1972. A chiral cystine disulfide group without inherent optical activity in the long-wavelength region (1H- and 13C- NMR, UV, CD, ORD studies with cyclo-L-cystine). *Helv Chim Acta 55*:947–961.

Dreyfus LA, Harville B, Howard DE, Shaban R, Beatty DM, Morris SJ. 1993. Calcium influx mediated by the *Escherichia coli* heat-stable enterotoxin B (ST_B). *Proc Natl Acad Sci USA 90*:3202–3206.

Dreyfus LA, Urban RG, Whip SC, Slaughter C, Tachias K, Kupersztoch YM. 1992. Purification of the STb enterotoxin of *Escherichia coli* and the role of selected amino acids on its secretion, stability and toxicity. *Mol Microbiol 6*:2397–2406.

Fesik SW, Zuiderweg RP. 1990. Heteronuclear three-dimensional NMR spectroscopy of isotopically labeled biological macromolecules. *Q Rev Biophys 23*:97–131.

Field ML, Graf LH, Laird WJ, Smith PL. 1978. Heat-stable enterotoxin of *Escherichia coli*: In vitro effects of guanylate cyclase activity, cGMP concentration, and ion transport in small intestine. *Proc Natl Acad Sci USA 75*:2800–2804.

Fujii Y, Okamuro Y, Hitotsubashi S, Saito A, Akashi N, Okamoto K. 1994. Effect of alterations of basic amino acid residues of *Escherichia coli* heat-stable enterotoxin II on enterotoxicity. *Infect Immunol 62*:2295–2301.

Gariépy J, Judd AK, Schoolnik GK. 1987. Importance of disulfide bridges in the structure and activity of *Escherichia coli* enterotoxin ST1b. *Proc Natl Acad Sci USA 84*:8907–8911.

Gariépy J, Lane A, Frayman F, Wilbur D, Robien W, Schoolnik GK, Jardetzky O. 1986. Structure of the toxin domain of the *Escherichia coli* heat stable enterotoxin STI. *Biochemistry 25*:7854–7866.

Gilquin B, Roumestand C, Zinn-Justin S, Menez A, Toma F. 1993. Refined three-dimensional solution structure of a snake cardiotoxin: Analysis of the side-chain organization suggests the existence of a possible phospholipid binding site. *Biopolymers 33*:1659–1675.

Griesinger C, Otting G, Wüthrich K, Ernst RR. 1988. Clean TOCSY for 1H spin system identification in macromolecules. *J Am Chem Soc 110*:7870–7872.

Guérrant RL, Hughes JM, Chang B, Robertson DC, Murad F. 1980. Activation of intestinal guanylate cyclase by heat-stable enterotoxin of *Escherichia coli*: Studies of tissue specificity, potential receptors, and intermediates. *J Infect Dis 142*:220–227.

Harville BA, Dreyfus LA. 1995. Involvement of 5-hydroxytryptamine and prostaglanidin E2 in the intestinal secretory action of *Escherichia coli* heat-stable enterotoxin B. *Infect Immunol 63*:745–750.

Havel TF. 1991. An evaluation of computational strategies for use in the determination of protein structure from distance constraints obtained by nuclear magnetic resonance. *Prog Biophys Mol Biol 56*:43–78.

Havel TF, Kuntz ID, Crippen GM. 1983. Theory and practice of distance geometry. *Bull Math Biol 45*:665–720.

Jeener J, Meier BH, Bachmann P, Ernst RR. 1979. Investigation of exchange processes by two-dimensional NMR spectroscopy. *J Chem Phys 71*:4546–4553.

Johnson BA, Sugg EE. 1992. Determination of the 3-dimensional structure of iberiotoxin in solution by H-1 nuclear magnetic resonance spectroscopy. *Biochemistry 31*:8151–9159.

Karplus PA, Schulz GE. 1987. Refined structure of glutathione reductase at 1.54 Ångstroms resolution. *J Mol Biol 195*:701.

Kumar A, Wagner G, Ernst RR, Wüthrich K. 1981. Buildup rates of the nuclear Overhauser effect measured by two-dimensional proton magnetic resonance spectroscopy: Implication for studies of protein conformation. *J Am Chem Soc 103*:3654–3658.

Kuntz ID, Thomason JF, Oshiro CM. 1989. Distance geometry. *Methods Enzymol 177*:159–204.

Kupersztoch YM, Tachias K, Moomaw CR, Dreyfus LA, Urban R, Slaughter C, Whipp S. 1990. Secretion of methanol-insoluble heat-stable enterotoxin (STb): Energy- and secA-dependent conversion of Pre-STb to an intermediate indistinguishable from the extracellular toxin. *J Bacteriol 172*:2427–2432.

Le Du MH, Marchot P, Bougis PE, Fontecilla-Camps JC. 1992. 1.9 Ång-

strom resolution structure of fasciculin 1 an anti-acetylcholinesterase toxin from green mamba snake toxin. *J Biol Chem 267*:22122-22130.

Lee CH, Moseley SL, Moon HW, Whipp SC, Gyles CL, So M. 1983. Characterization of the gene encoding heat-stable toxin II and preliminary molecular epidemiological studies of enterotoxigenic *Escherichia coli* heat-stable toxin II producers. *Infect Immunol 42*:264-268.

Leszczynski JF, Rose GD. 1986. Loops in globular proteins: A novel category of secondary structure. *Science 234*:849-855.

Maniatis T, Fritsch EF, Sambrook J, eds. 1982. *Molecular cloning: A laboratory manual.* Cold Spring Harbor, New York: Cold Spring Harbor Laboratory Press.

Marion D, Driscoll PC, Kay LE, Wingfield PT, Bax A, Gronenborn AM, Clore GM. 1989a. Overcoming the overlap problem in the assignment of ^{1}H NMR spectra of larger proteins by use of three-dimensional heteronuclear ^{1}H-^{15}N Hartmann-Hahn-multiple quantum coherence and nuclear Overhauser-multiple quantum coherence spectroscopy: Application to interleukin 1β. *Biochemistry 28*:6150-6156.

Marion D, Ikura M, Bax A. 1989b. Improved solvent suppression in one- and two-dimensional NMR spectra by convolution of time-domain data. *J Magn Reson 84*:425-430.

Marion D, Kay LE, Sparks SW, Torchia DA, Bax A. 1989c. Three-dimensional heteronuclear NMR of ^{15}N-labeled proteins. *J Am Chem Soc 111*:1515-1517.

Messerle BA, Wider G, Otting G, Weber C, Wüthrich K. 1989. Spin lock in 2D and 3D NMR spectroscopy with H_2O solutions. *J Magn Reson 85*:608-613.

Meunier S, Bernassau JM, Sabatier JM, Martin-Eauclaire MF, Van Rietschoten J, Cambillau C, Darbon H. 1993. Solution structure of P05-NH2, a scorpion toxin analog with high affinity for the apamin-sensitive potassium channel. *Biochemistry 32:11969-11976.*

Oswald RE, Sutcliffe MJ, Bamberger M, Loring RH, Braswell E, Dobson CM. 1991. Solution structure of neuronal bungarotoxin determined by two-dimensional NMR spectroscopy: Sequence specific assignments, secondary structure, and dimer formation. *Biochemistry 30*:4901-4909.

Ozaki H, Sato T, Kubota H, Hata Y, Katsube Y, Shimonishi Y. 1991. Molecular structure of the toxin domain of heat-stable enterotoxin produced by a pathogenic strain of *Escherichia coli*. A putative binding site for a binding protein on rat intestinal epithelial cell membranes. *J Biol Chem 266*:5934-5941.

Pardi A, Zhang XL, Selsted ME, Skalicky JJ, Yip PF. 1992. NMR studies of defensin antimicrobial peptides. 2. 3-Dimensional structures of rabbit NP-2 and human HNP-1. *Biochemistry 31*:11357-11364.

Picken RN, Mazaitis AJ, Maas WK, Rey M, Heyneker H. 1983. Nucleotide sequence of the gene for heat-stable enterotoxin II of *Escherichia coli*. *Infect Immunol 42*:269-275.

Provencher SW. 1982. CONTIN: A general purpose constrained regularization program for inverting noisy linear algebraic and integral equations. *Comput Phys Commun 27*:229-242.

Provencher SW, Glockner J. 1981. Estimation of globular protein secondary structure from circular dichroism. *Biochemistry 20*:33-37.

Ramachandran GN, Sasisekharan V. 1968. Conformation of polypeptides and proteins. *Adv Protein Chem 28*:283-437.

Rasheed K, Guzman-Verduzco LM, Kupersztoch YM. 1990. Two precursors of heat-stable enterotoxin of *Escherichia coli*: Evidence of extracellular processing. *Mol Microbiol 4*:265-274.

Rees B, Bilwes A, Samama JP, Moras D. 1990. Cardiotoxin VII4 from *Naja mossambica mossambica*: The refined crystal structure. *J Mol Biol 214*:281-297.

Sack RB. 1975. Human diarrheal disease caused by enterotoxigenic *E. coli*. *Annu Rev Microbiol 29*:333-353.

Schagger H, von Jagow G. 1987. Tricine-sodium dodecyl sulfate-polyacrylamide gel electrophoresis for the separation of proteins in the range from 1 to 100 kDa. *Anal Biochem 166*:368-379.

Schulz S, Green CK, Yuen PST, Garbers D. 1990. Guanylyl cyclase is a heat-stable enterotoxin receptor. *Cell 63*:941-948.

Shimonishi Y, Hidaka Y, Koizumi M, Hane M, Aimoto S, Takeda T, Miwatani T, Takeda Y. 1987. Mode of disulfide bond formation of a heat-stable enterotoxin (STh) produced by a human strain of enterotoxigenic *Escherichia coli*. *FEBS Lett 215*:165-170.

States DJ, Haberkon RA, Ruben DJ. 1982. A two-dimensional nuclear Overhauser experiment with pure absorption phase in four quadrants. *J Magn Reson 48*:286-292.

Teeter MM. 1984. Water structure of a hydrophobic protein at atomic resolution. Pentagon rings of water molecules in crystals of crambin. *Proc Natl Acad Sci USA 81*:6014-6018.

Urban RG, Pipper EM, Dreyfus LA, Whipp SC. 1990. High-level production of *Escherichia coli* STb heat-stable enterotoxin and quantification by a direct enzyme-linked immunosorbent assay. *J Clin Microbiol 28*: 2383-2388.

Whipp SC. 1990. Assay for the enterotoxigenic *Escherichia coli* heat-stable toxin b in rats and mice. *Infect Immunol 58*:930-934.

Whipp SC, Moon HW, Argenzio RA. 1981. Comparison of enterotoxic activities of heat-stable enterotoxins from class 1 and class 2 *Escherichia coli* of swine origin. *Infect Immunol 31*:245-251.

Widmer H, Billeter M, Wüthrich K. 1989. Three-dimensional structure of the neurotoxin ATX 1A from *Anemonia sulcata* in aqueous solution determined by nuclear magnetic resonance spectroscopy. *Proteins Struct Funct Genet 6*:357-371.

Wishart DS, Sykes BD, Richards FM. 1992. The chemical shift index—A fast and simple method for the assignment of protein secondary structure through NMR spectroscopy. *Biochemistry 31*:1647-1651.

Xu X, Nelson JW. 1993. Solution structure of tertiapin determined using nuclear magnetic resonance and distance-geometry. *Proteins Struct Funct Genet 17*:124-137.

Yu C, Bhaskaran R, Chuang LC, Yang CC. 1993a. Solution conformation of cobrotoxin—A nuclear magnetic resonance and hybrid distance geometry dynamical simulated annealing study. *Biochemistry 32*:2131-2136.

Yu H, Rosen MK, Saccomano NA, Phillips D, Volkmann RA, Schreiber SL. 1993b. Sequential assignment and structure determination of spider toxin ω-Aga-1VB. *Biochemistry 32*:13123-13129.

Zuiderweg ERP, Fesik SW. 1989. Heteronuclear three-dimensional NMR spectroscopy of the inflammatory protein C5A. *Biochemistry 28*:2387-2391.